Regionalization in Fine-Grid GFS MOS 6-h Quantitative Precipitation Forecasts

JEROME P. CHARBA AND FREDERICK G. SAMPLATSKY

NOAA/National Weather Service, Meteorological Development Laboratory, Silver Spring, Maryland

(Manuscript received 5 January 2009, in final form 31 August 2009)

ABSTRACT

The recent emergence of the National Digital Forecast Database as the flagship product of the National Weather Service has resulted in an increased demand for forecast guidance products on fine-mesh grids. Unfortunately, fine-grid forecasts with geographically regionalized statistical models are usually plagued by nonmeteorological discontinuities at regional boundaries. This study treats the problem in a regionalized Global Forecast System (GFS)-based model output statistics (MOS) application that produces 6-h probabilistic quantitative precipitation forecasts (PQPFs) on a 4-km grid up to 192 h in advance. The technique involves incorporating areal overlap in the geographical regionalization and weighting multiple PQPFs in region-overlap zones. The degree of overlap ranges from about 20 km along meteorologically significant regional boundaries to about 150 km at quasi-arbitrary boundaries. The forecast-weighting constants for a grid point in an overlap zone vary in direct proportion to the distances to the closest associated regional boundaries.

The application of the region-overlap and forecast-weighting techniques resulted in retention of sharp PQPF gradients along meteorologically significant regional boundaries and prevention of artificial discontinuities at quasi-arbitrary boundaries. The eradication of the discontinuities in the forecast patterns was achieved without sacrificing forecast skill. While the regionalization was customized for producing high-spatial-resolution 6-h PQPFs over the contiguous United States with a specialized gridded MOS application, the region-overlap and forecast-weighting techniques may have general applicability. Also, the quality of the 6-h PQPFs was not strongly dependent on customization of the regionalization.

1. Introduction

Over the history of statistical prediction of sensible weather elements, the forecasts, in most applications, have been issued at irregularly spaced stations (Glahn and Lowry 1972; Carter et al. 1989), as the predictands have been furnished by conventional surface observations. On the other hand, since the 1970s severe local storm reports and digitized weather radar observations have been used for analogous grid-based applications (Charba 1977, 1979; Reap and Foster 1979), whereby the predictors and predictands (forecasts) are specified at grid points instead of stations.[1] Such grid applications were expanded in the 1980s and beyond with the availability of remotely sensed lightning strike data (e.g., Reap 1991; Hughes 1999, 2004; Charba and Liang 2005) and grid usage of cooperative observer station reports (Charba 1987, 1998).

Grid-based statistical model applications have significant advantages over station-based analogs. Specifically, the grid approach 1) provides uniform spatial resolution in the forecasts over the coverage domain, 2) allows for the full spatial resolution in predictor–predictand data to be included in the forecasts, and 3) supports production of highly informative graphical displays of the forecasts, each of which should enhance the quality and utility of the forecast products. Note that the recent emergence of the (gridded) National Digital Forecast Database (Glahn and Ruth 2003) as the flagship product of the National Weather Service (NWS 2007, p.7) has resulted in an increased demand for forecast guidance on fine-mesh grids. In fact, this added demand has resulted in the recent implementation of grid rendering of station-oriented model output statistics (MOS; Glahn and Lowry 1972) forecasts on a fine-mesh grid via special objective analysis techniques (Glahn et al. 2009).

[1] Note that statistical prediction equations could be developed from one set of points and then applied to another set. Thus, the equations could be developed from station data and then applied (forecasts issued) on a grid.

Corresponding author address: Jerome P. Charba, National Weather Service, 1325 East-West Highway, Silver Spring, MD 20910-3283.
E-mail: jerome.charba@noaa.gov

DOI: 10.1175/2010MWR2926.1

A widely used approach in statistical forecast applications at the Meteorological Development Laboratory involves geographically regionalized prediction equations. With this technique, a ''regionalized operator'' (RO; Lowry and Glahn 1976) is used to develop and apply a single statistical prediction equation to multiple points (a ''geographical region'') within the overall model domain; a unique equation applies to each region. This technique is generally used to generate statistically reliable samples for rare-event predictands, which may not be possible with a ''single station'' approach (Carter et al. 1989). In the extreme case of RO, a single equation applies to the entire coverage domain, which is referred to as a ''national'' model in this article. However, forecast skill may be reduced since optimized predictors usually exhibit geographical variations in response to corresponding variations in physical processes associated with the predictand. A good example of regional variations in physical processes for precipitation occurrence is the predominance of orographic mechanisms in steep mountainous areas versus cyclonic mechanisms in plains areas. Also, when the statistical model consists of a MOS application (Glahn and Lowry 1972; Carter et al. 1989), a regional approach should be superior if the driving numerical weather prediction (NWP) model contains geographical variations in systematic forecast error (bias).

On the other hand, a significant ''forecast mapping'' problem may arise with grid-oriented, regionalized statistical models. Spatial discontinuities in the forecasts, which do not have a meteorological basis, may appear along the regional boundaries. Such artificial discontinuities result in incoherent forecast map patterns, which could severely hinder their guidance utility. This problem was not serious in the early gridded model applications, as the grids were relatively coarse (~80 km) and discontinuities could be mitigated with conventional grid smoothing. When the grid resolution is increased to, say, 20 km, such smoothing may no longer be an effective treatment, and the severity of the problem increases with even finer grids. It is important to note that such regional inconsistency in statistical forecasts may arise even with the common station-oriented approach. However, the problem may be poorly recognized or even undetected because the station forecasts are not often mapped.

In a concurrent article, Charba and Samplatsky (2011, hereinafter CS) describe a regionalized MOS application that produces 6-h probabilistic quantitative precipitation forecasts (PQPFs) on a fine-mesh grid. Very briefly, the 6-h PQPFs are produced by geographically stratified multiple linear regression equations, where the predictand consists of multiple cumulative precipitation categories in binary form. The precipitation categories were specified from quality-controlled[2] ''stage IV'' mosaics (information online at http://www.emc.ncep.noaa.gov/mmb/ylin/pcpanl/stage4/) of regional ''stage III'' 6-h precipitation analyses on a 4-km grid; the stage III precipitation grids (Fulton et al. 1998; Henkel and Peterson 1996) are produced at NWS River Forecast Centers. The PQPF predictor variables were also specified on the 4-km grid from large-scale forecast output from the National Centers for Environmental Prediction (NCEP) Global Forecast System (GFS; Kanamitsu et al. 1991; Iredell and Caplan 1997) together with multiple finescale precipitation climatologies and topography (topoclimatology). In the predictor development, specialized derived predictors (called interactive predictors in CS) were used to effectively transfer fine spatial details in the topoclimatic data into the large-scale GFS model output variables (and ultimately into the PQPFs). The 6-h PQPFs are valid for projections in the 12–84-h range from the 0000 and 1200 UTC cycles. (One of several subsequent upgrades to the model described in CS has extended the forecast projections to 192 h.) Several additional precipitation products described in CS are derived from the PQPFs (CS).

Based on the lead author's previous experience with statistical forecast applications involving fine grids and geographically regionalized regression equations, the problem of artificial discontinuities in the forecasts along the regional boundaries was anticipated. Indeed, the problem arose with 6-h PQPF regression equations developed with conventional regionalization procedures. This article is organized by first examining the nature of the discontinuity problem (section 2), then treating it by modifying the regionalization (section 3), and, finally, applying the newly regionalized regression equations (section 4). In section 5, PQPF performance with the new regionalization is compared with both the conventional regionalization and nonregionalized (''national'') approaches. Section 6 contains a discussion of our findings and several model sensitivity experiments with the new method, and section 7 contains a summary and comments.

2. Regional discontinuities: Posing the problem

a. Specification of discrete regions

The regions used for geographically stratifying the initial PQPF regression equations were formed by partitioning the conterminous United States (CONUS)

[2] The quality-control procedures are summarized in CS.

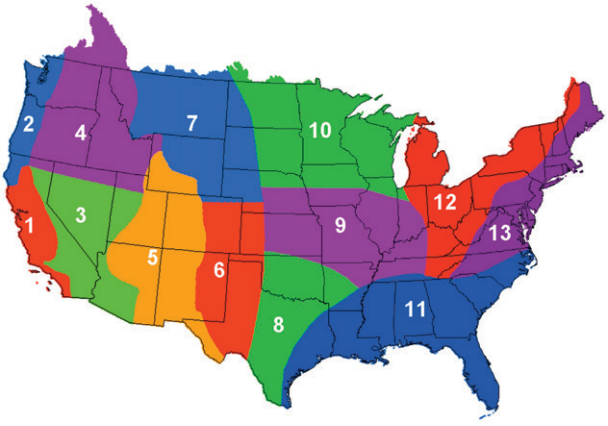

FIG. 1. Developmental domain and "discrete" geographical regions into which it was partitioned (region numbers are referred to in the text).

developmental domain[3] into the 13 subareas shown in Fig. 1. These subareas, called discrete regions in this article, were specified on the basis of several considerations, which include perceived geographical variations in precipitation forcing mechanisms, regional bias error in GFS model predictors, objective and subjective PQPF performance assessments, and development/application cost of the statistical model. Among these factors, perceived precipitation controls were primary, and they were subjectively inferred mainly from finescale topography and precipitation climatology (monthly and seasonal) maps.

The topography and precipitation climatology fields were developed on the 4-km grid, as detailed in CS. Very briefly, 30-arc-s terrain elevation data from the U.S. Geological Survey were interpolated to this grid. Among the three types of gridded precipitation climatologies applied, one consisted of monthly mean relative frequencies for multiple 6-h precipitation categories stratified by the time of the day (Charba et al. 1998), another consisted of Parameter-elevation Regressions on Independent Slopes Model (PRISM) monthly mean precipitation (Daly et al. 1994), and the third consisted of warm and cool season relative frequencies for the eight 6-h precipitation thresholds that composed the predictands (section 1). The seasonal relative frequencies were computed at each 4-km grid point by combining the predictand data over the four standard 6-h time periods (to increase the sample size). Finally, spatial smoothing was applied to each of the above gridded topoclimatic data types such that the smallest resolved scale was about 20 km.

To illustrate how precipitation controls were deduced from these topoclimatic grids, Fig. 2a shows a map of the terrain elevation and Fig. 2b shows the cool season relative frequency of 6-h precipitation $\geq$0.10 in. (a heavily used climatology map). In the western United States, the alignment of principal features in the relative frequencies along slopes of the Coastal, Sierra, Cascade, and Rocky Mountain ranges implies that orography is a dominant precipitation mechanism during the cool season. In this western area, the winding regional boundaries oriented roughly north south in Fig. 1 reflect the orographic effects. Specifically, the positioning of these boundaries along the major mountain crests aims to separate precipitation maxima along the western (windward) slopes from the minima along eastern (lee) slopes. This boundary positioning should act to preserve the precipitation contrasts in statistical samples taken from the delineated regions. Thus, these regional boundaries are referred to as natural boundaries. In the eastern United States, the broad precipitation frequency maximum oriented southwest–northeast in Fig. 2b suggests that cyclonic systems, which develop east of the Rocky Mountains and then travel northeastward, is the dominant cool season precipitation mechanism. The smooth region boundaries oriented southwest–northeast were drawn to reflect this precipitation mechanism. The more irregular boundary that separates regions 12 and 13 (Fig. 1) is positioned along the crest of the eastern mountain ranges (Fig. 2a) in order to capture possible orographic effects. Even though precipitation relative frequency gradients along the mountain slopes there are quite weak[4] (Fig. 2b), this regional boundary is also considered a natural boundary.

The placement of the remaining boundaries in Fig. 1 was more arbitrary, as the primary influences on precipitation for their locations were believed to reside mostly at large scales. One guide for placing these "quasi arbitrary" boundaries was to separate geographical areas with large-scale latitudinal variations in the climatology of the heavier precipitation thresholds (not shown), which accounts for many of the east–west boundaries. Other boundaries were positioned to separate areas that were (a) characterized by elevated nonmountainous terrain (regions 6 and 7), (b) located downwind of large lakes

[3] The developmental domain consists of the coverage area of the stage IV precipitation data shown in Fig. 1. All results presented in this article pertain to this restricted coverage area. For real-time application of the statistical model, the coverage is expanded to fill gaps (such as the Great Lakes) and extend the perimeter beyond the CONUS borders (CS).

[4] The absence of clear evidence of orographic precipitation effects in the eastern United States in Fig. 2b could result from comparable terrain slope enhancement (or suppression) of precipitation on both the eastern and western slopes of the mountains there.

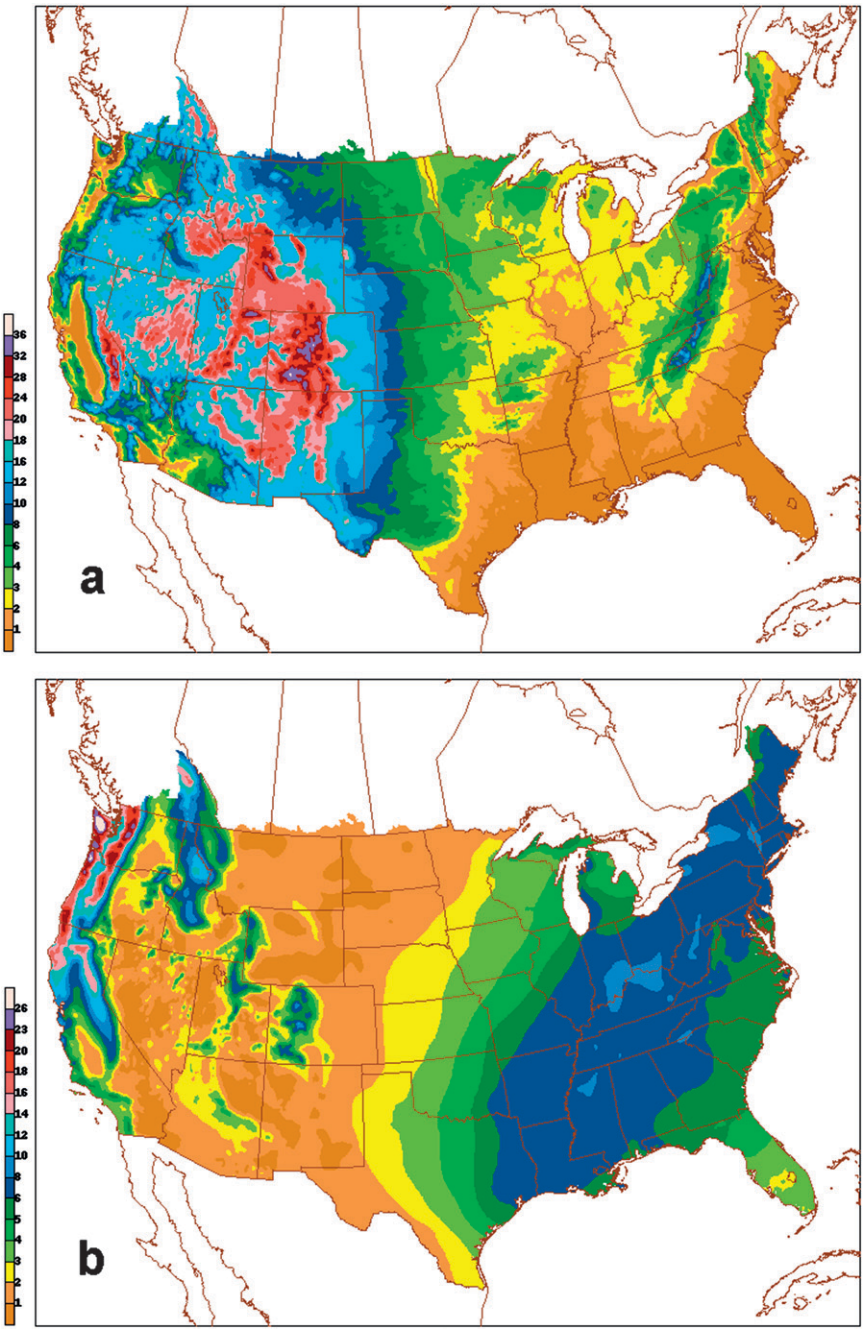

FIG. 2. (a) Terrain elevation (hundreds of meters) and (b) cool season (October–March) mean relative frequency (%) of 6-h precipitation of ≥0.10 in.

(region 12), or (c) bounded by ocean coasts (regions 1, 2, 11, and 13).

It is noted that although possible geographical variations in systematic error (bias) in the GFS model output were not directly considered in the specification of the regions, an objective test was performed to see whether such error was present in GFS precipitation forecasts (the most important single PQPF predictor; CS). Specifically, bias scores for GFS precipitation forecasts, averaged within each of the regions in Fig. 1, were computed. In the experiment, the GFS precipitation was first converted into the eight categorical (binary) variables used as predictands in this study. Then, the regional bias was computed separately for each precipitation category,

each of four ''day 2'' projections (30, 36, 42, and 48 h), and each of the two seasons over the full historical sample (January 2001–March 2008) used in this study. We found (results not shown) negligible variation in bias over the regions at all precipitation thresholds during both the warm (April–September) and cool (October–March) seasons. This result suggests that a concerted effort to factor GFS bias into the regions specification, at the scale of the regions in Fig. 1, would have had little value.

Note, however, that the above finding should not be taken to imply that geographical variations in bias in GFS precipitation forecasts do not exist. Indeed, they probably do exist, but not for the scale in which geographical regionalization was feasible in this study. For instance, maps of GFS precipitation forecasts were visually inspected for many cases over the sampling period. We found that for the western United States the smallest spatial scales resolved in the precipitation forecasts were substantially larger than the scales resolved in the precipitation climatology fields (which were used to define the regions; see Figs. 1 and 2b). Over the eastern United States the resolved scales in the GFS precipitation forecasts were similar to the large-scale precipitation climatology features, but the more minor small-scale precipitation climatology variations associated with the mountains and Great Lakes were poorly resolved (Fig. 2b).

These findings, taken together, suggest that significant geographical bias variations in GFS 6-h precipitation forecasts (if they exist at all) occur on smaller scales than those resolvable by the relatively large regions used in this study. For instance, to resolve such small-scale bias, a separate region would probably be needed for each windward and lee slope of each significant mountain chain [e.g., as incorporated into the precipitation climatology mapping procedures used in Daly et al. (1994)]. Further, an endeavor to incorporate such fine regionalization into MOS procedures (Carter et al. 1989) might require building a long history of ''reforecasts'' with a frozen NWP model [see Hamill et al. (2008)].

b. *Development and application of conventionally regionalized PQPF regression equations*

The standard MOS approach (Glahn and Lowry 1972) was used for development and application of regionalized PQPF regression equations based on the regions in Fig. 1. The predictand consists of eight cumulative categories of 6-h precipitation ($\geq$0.01, $\geq$0.10, $\geq$0.25, $\geq$0.50, $\geq$0.75, $\geq$1.00, $\geq$1.50, and $\geq$2.00 in.), and the predictors were specified from GFS model output together with the topography and multiple precipitation climatologies noted in the previous subsection. The developmental sample of paired predictor–predictand data, for a given region in Fig. 1, was formed by combining data from all 4-km grid points within the region over the developmental period consisting of all days from January 2001 to March 2007. The samples were stratified by 6-month warm (April–September) and cool (October–March) seasons, and the ensuing regression equations were applied to corresponding independent samples from the period April 2007 to March 2008.[5]

The defining properties of 6-h PQPFs from these conventionally regionalized regression equations are illustrated for a case selected from the independent sample. Figure 3a shows a cool season example of a 36-h PQPF of $\geq$0.10 in. valid for the 6-h period ending 0000 UTC 30 January 2008, and Fig. 3d contains the verifying quality-controlled stage IV 6-h precipitation analysis. These maps show that in the western United States the fine spatial scales in the forecast and observed fields match well. Over the eastern United States, on the other hand, the forecast field is much smoother than the observed. More significantly, the PQPF pattern is severely marred by nonmeteorological discontinuities along regional boundaries (Fig. 1), even though the PQPF field had been smoothed with a weighted nine-point filter (Shuman 1957). The discontinuities are especially severe in Arkansas, Indiana, and Illinois, with more minor examples in Tennessee and Pennsylvania. The absence of such nonmeteorological discontinuities in the western United States in this case arises mainly because most regional boundaries in the area of high probabilities are natural boundaries (section 2a).

The artificial PQPF discontinuities in Fig. 3a result from independent derivation of the regression equations among the individual regions. More specifically, they stem from regional variations in the predictor variables and regression coefficients (CS) as well as from regional variations in the precipitation predictability (evidenced by regional performance scores presented in section 5) and the sample precipitation climatology. In fact, the

[5] Note that forecast performance with an MOS application can suffer when the driving NWP model undergoes significant changes (Carter et al. 1989). Since the GFS underwent a number of changes (information online at http://www.emc.ncep.noaa.gov/gmb/STATS/html/model_changes.html) over the relatively long sampling period used in this study, a valid concern is whether the changes may have substantially affected its (statistical) forecast performance (i.e., statistical stability of the sample). As a check for this, we computed separate domain-wide threat [same as CSI; Schaefer (1990)] and bias scores for categorized GFS precipitation forecasts over the first and last halves of the sampling period. The results showed only a very slight change (improvement) in the scores from the first half-sample to the second (not shown), which was not cause for concern.

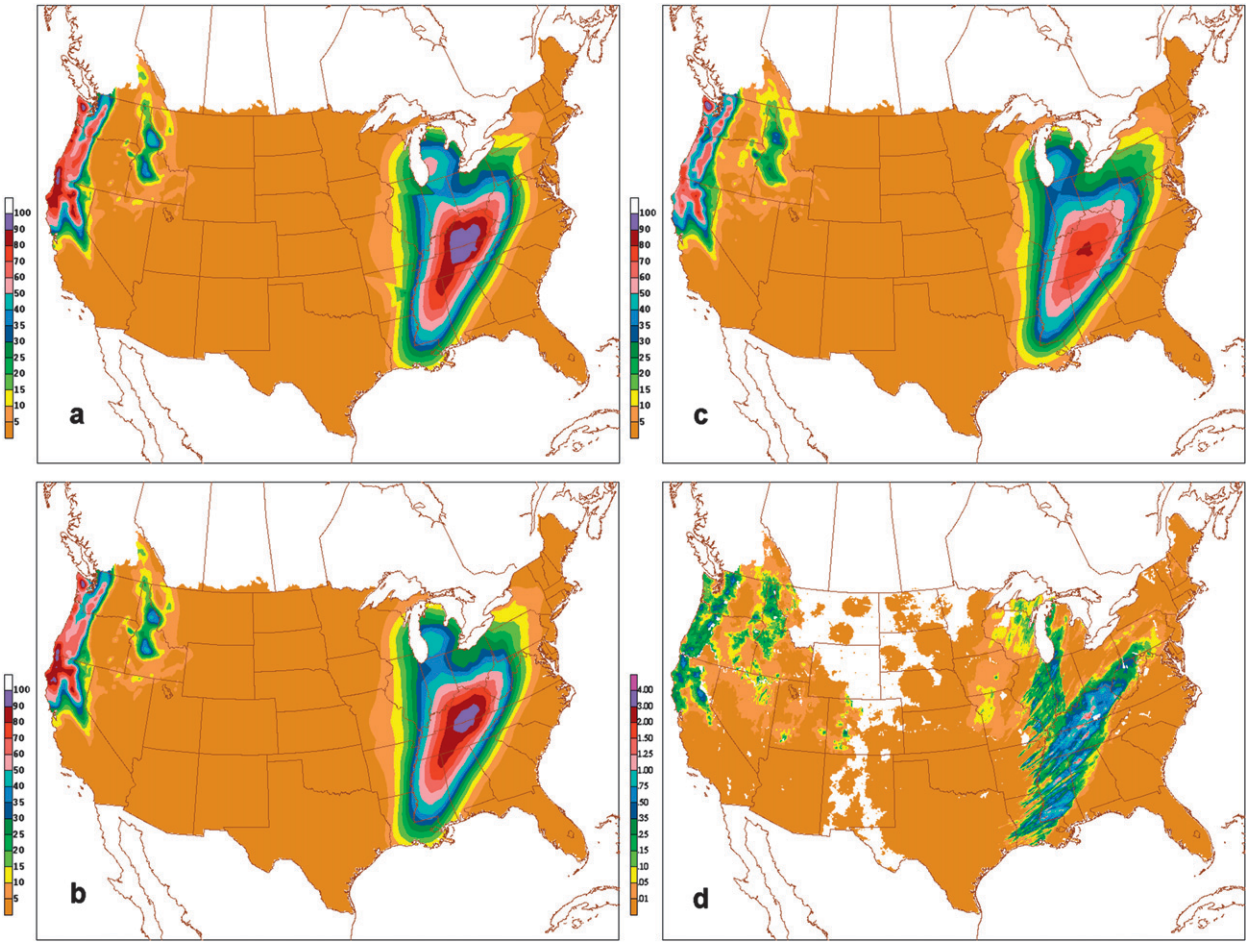

FIG. 3. Smoothed 36-h forecast probability (%) of ≥0.10 in. for the 6-h period ending 0000 UTC 30 Jan 2008 produced with the (a) discrete regions, DRG; (b) overlapping regions, ORG; and (c) national models, NAT. (d) Quality-controlled stage IV 6-h precipitation analysis (in.) for the valid period. [Irregular over-land white areas indicate missing data, which result from supplemental quality control of the precipitation data performed at the NWS Meteorological Development Laboratory (CS).]

notion that sample climatology was a factor is supported by the finding that the most intense artificial discontinuities in Fig. 3a appear along the large-scale spatial gradient in precipitation relative frequencies that stretches from central Texas to Lake Michigan (Fig. 2b). Discontinuities similar to those present in this case appeared in many other cases examined, and also with regression equations involving variations in the regions specification from that in Fig. 1 (not shown).[6] If left untreated, the discontinuity problem would likely undermine the credibility of the PQPF guidance.

Of course, the discontinuity problem can be avoided entirely with a ''national equation'' approach, whereby a single regression equation (for a given precipitation category and forecast projection) applies to the entire CONUS domain. In fact, this simple approach was recently applied for 3-h MOS thunderstorm probability prediction over the CONUS with a 20-km grid (Hughes 2004), but the degree to which forecast skill may have been sacrificed was not addressed. Thus, for comparative testing against the regionalized PQPF model discussed above, we developed and applied a comparable national model. To ensure strict comparability with the regional counterpart, the development and application of the national regression equations (including smoothing applied to PQPF fields) were identical.

The smoothed 6-h PQPF field obtained with the national model corresponding to Fig. 3a is shown in Fig. 3c. A comparison of the two PQPF fields reveals several

[6] Also, a similar discontinuity problem appeared in the lead author's previous gridded regionalized statistical forecast applications involving short-range (<24 h) QPF (Charba 1998) and thunderstorm (Charba and Liang 2005) predictands with a (relatively coarse) 20-km grid. As the discontinuity problem in these applications was relatively mild, it was not documented.

notable differences, of which the most obvious is that nonmeteorological discontinuities are not present with the national model. On the other hand, the regional model PQPF field exhibits enhanced pattern features, which include higher peak values and improved sharpness (probabilities are more clustered toward either 0 or high values). Excluding the regional discontinuities, the regional model also exhibits slightly better spatial coherency over the eastern United States; the noticeable spatial incoherency with the national model in this area may be due to inappropriate (nationally averaged) contributions from high-spatial-resolution topoclimatic predictors in the underlying PQPF regression equation.

Excluding the discontinuities, the superior PQPF properties with the regional model indicated in Fig. 3a were evident in many similar comparisons from both seasons and all precipitation thresholds and forecast projections. Improved forecast performance with the regional model over the national model was also evident from objective comparative scoring (presented in section 5). Thus, the challenge posed for reformulating the regional model was to mitigate the PQPF discontinuities, but still retain its improved forecast performance properties.

3. Specification of overlapping geographical regions

The approach we took to treat the problem of the PQPF discontinuities with the discrete regions (Fig. 1) was to introduce overlap between neighboring regions. The rationale behind the approach is that it would introduce a measure of consistency among the regional regression equations because of the sample sharing in the overlap areas. The strategy used to implement the concept was to outwardly expand the previously specified discrete region boundaries (section 2a).

Several principles were used to guide the expansion of each discrete region. 1) The degree of the overlap among the regions should be minimized to maximize regional uniqueness in the regression equations. 2) The overlap for natural boundaries should be less than that for quasi-arbitrary boundaries to support preservation of spatial precipitation gradients that characterize the former. 3) Among natural boundaries, the overlap should be inversely related to the boundary strength, where the latter is directly related to the intensity of the spatial gradients in the terrain elevation and precipitation relative frequencies.

An important aspect of the overlap specification for natural boundaries (of varying strength) involved assigning the overlap extent. For quasi-arbitrary boundaries, a relatively broad, fixed overlap extent was used. For both types of boundaries, the overlap extent was determined largely on the basis of the appearance of the PQPF map patterns for selected heavy precipitation cases, as varying trial overlap specifications were found to have a negligible impact on an objective measure of PQPF skill (described in section 5). Thus, the specification of the overlap extent was mostly subjectively determined, where key considerations were the assurance that (a) PQPF gradients were consistent with climatic precipitation gradients across natural boundaries and (b) artificial PQPF gradients were suppressed along quasi-arbitrary boundaries.

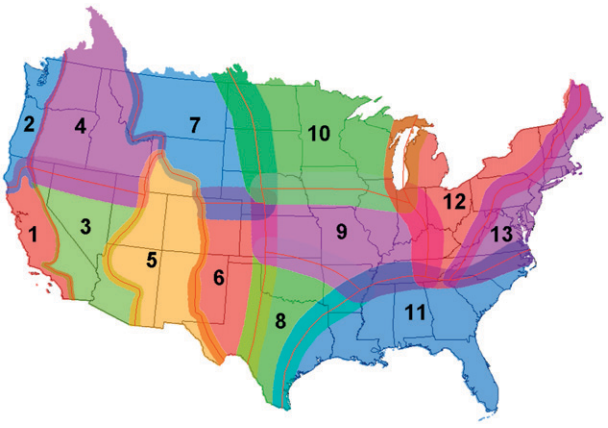

FIG. 4. Overlapping regions, with discrete regional boundaries (light red lines) and region numbers superimposed. With transparent shading used to show the overlap of neighboring regions, the full extent of an overlap region is the nonoverlapping core plus the overlap along the periphery.

The overlap regions obtained through this empirical process are shown in Fig. 4. Among natural boundaries the overlap distances range from a minimum of about 20 km for the strong natural boundary separating regions 1 and 2 from 3 and 4 to 100 km for the weak natural boundary that separates regions 12 and 13. The moderate intensity natural boundaries that extend from western Montana and terminate in either southern Arizona or West Texas exhibit overlap in the 30–50-km range. These relatively narrow overlaps contrast strongly with the broad overlap bands for the quasi-arbitrary boundaries, where the overlap averaged 150 km. [The region overlap was specified manually with the aid of a geographical information system (GIS) software package. The overlapping region boundaries were drawn with a mouse on a geographical background map, and then the grid points falling inside each overlapping region (GIS shapefile) were extracted. Thus, it is convenient to express the overlap in terms of map distances rather than, say, by the number of grid points.]

A noteworthy aspect of the overlapping regions is the "overlap level," which, for a given location, is the number

of regions that share the overlap. Examination of Fig. 4 reveals that most of the overlap zones are common to just two regions (“level 2” overlap). The opposite extreme consists of level 4 overlap (involving regions 6, 7, 9, and 10), which appears in a small area in central Nebraska.

The discrete and overlap regions shown in Figs. 1 and 4, respectively, apply to the cool season since they were specified with cool season precipitation considerations. The specification of the overlap for the warm season regions was performed independently, since we recognized that warm season precipitation mechanisms in some areas of the CONUS are different than those for the cool season. For example, the predominant effect of mountains was assumed to change from orographic in the cool season to thermodynamic in the warm season. Nevertheless, the regions that emerged were so similar to those for the cool season that separate sets were not justifiable. Thus, the regions described here were used for both the warm and cool season development of the PQPF model.

4. Application of the overlapping-regions regression equations

The development of PQPF regression equations based on the overlapping regions was identical to that for the discrete regions, except that the developmental samples were now formed from the expanded regions. As with the discrete regions, the sample for an overlap region was formed by pooling paired predictor–predictand data from all 4-km grid points falling within it. Otherwise, the development of the overlapping-regions regression equations was identical to that for the discrete regions.

The application of the overlapping-regions equations was also identical to that for discrete regions; that is, an equation was evaluated at each 4-km grid point within the applicable overlapping region. As this process is repeated for each overlapping region, a single PQPF value appears at the nonoverlap grid points and multiple PQPFs appear in overlap zones. Then, for a grid point in an overlap zone, the final PQPF (F) was computed as a weighted average of the multiple forecasts according to

$$F = \sum_{i=1}^{n} w_i F_i, \tag{1}$$

where w_i is the weight for region i, F_i is the corresponding PQPF value, and n is the number of regional PQPFs (two to four) at the point. Thus, to apply (1), suitable weight constant(s) at each grid point first had to be specified.

The weight value for an overlap point for a given region was defined to be directly proportional to the distance of the point to the closest (overlap) “internal boundary” for the region. The internal boundary is defined as that portion of the overall boundary perimeter that falls within the area of a neighboring region. For example, the weights w_1 and w_2 for a point overlapped by two regions (Fig. 5) are defined as

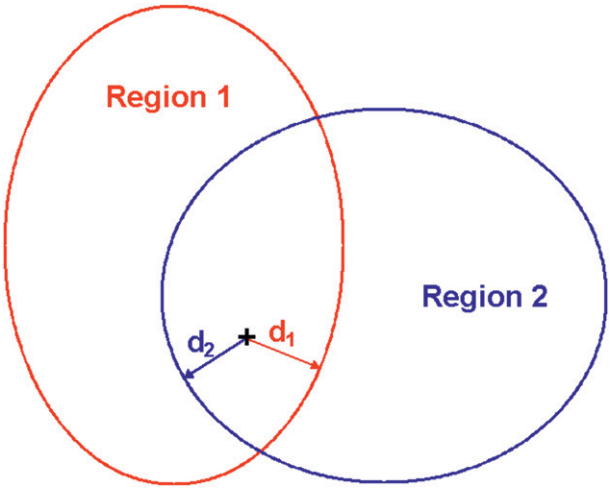

FIG. 5. Schematic of two overlapping regions (1 and 2). For a point within the overlap area, d_1 (d_2) is the closest distance of the point to the internal boundary of region 1 (region 2).

$$w_1 = \frac{d_1}{d_1 + d_2} \tag{2}$$

and

$$w_2 = \frac{d_2}{d_1 + d_2}, \tag{3}$$

where d_1 (d_2) is the closest distance to the internal boundary for region 1 (region 2). Note that

$$w_1 + w_2 = 1.$$

The weight specification is generalized for the case where the point is overlapped by n regions as

$$w_i = \frac{d_i}{\sum_{i=1}^{n} d_i}, \tag{4}$$

where w_i and d_i are defined for region i as before and

$$\sum_{i=1}^{n} w_i = 1.$$

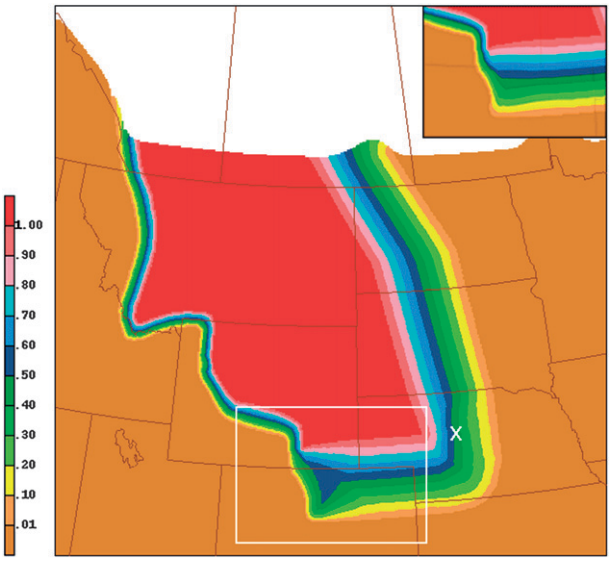

FIG. 6. Weight field for region 7. The weights outside the region have 0.0 values, and those within the rectangle (white lines) contain a small spurious feature, which is removed through manual editing in the inset (top right). For point "X," the four "level 4" weight values are noted in the text.

The weights were computed on the basis of (4) with a computer program. The data ingested into the program consisted of the grid locations for three sets of 4-km grid points: (a) all points in the CONUS domain (Fig. 1), (b) all points within each overlapping region, and (c) the internal boundary points for each overlapping region (Fig. 4). In a single run, the weight value for each grid point (overlap or otherwise) in each overlapping region was computed, and each regional weight field was stored for subsequent usage.

For illustration, the weight field for region 7 (Fig. 4) is shown in Fig. 6. Note that the weight values feature a "plateau" with a constant 1.0 value for the nonoverlapping portion of the region (Fig. 4), and, within overlap zones, the weights decrease smoothly to 0.0 at the regional perimeter. Note also that the weight gradient is much steeper along the western natural boundary than it is along the southern and eastern quasi-arbitrary boundaries. Finally, recall that region 7 was one of four regions that compose the level 4 overlap in central Nebraska (Fig. 4). The four weight values for a point denoted "X" in Fig. 6 are 0.059 for region 6, 0.450 for region 7, 0.236 for region 9, and 0.255 for region 10.

A noteworthy feature within the superimposed rectangle in Fig. 6 is a small perturbation in the weight field gradient where the weights have a fixed value of 0.5. The problem occurred because the overlap (internal) boundary for region 7 in this area is shared with the internal boundary for neighboring region 6 (Fig. 4). The shared boundary results in identical values for d_1 and d_2 in Fig. 5 and, thus, a 0.5 weight for both regions. This problem occurred in all regions where a narrow overlap zone (involving natural boundaries) intersected a wide overlap zone (involving quasi-arbitrary boundaries). Note that these "special overlap" intersections arose for regions 1, 2, 3, 4, 6, and 7 along a west-to-east band from northeast California to northern Colorado (Fig. 4). As for region 7, the perturbation in the weight field was small in each affected region. Thus, the problem did not have a significant negative impact on the ensuing PQPF fields, and its presence could have been ignored. On the other hand, since grid-editing software (Wier et al. 1998) was conveniently available, we chose to remove the minor perturbations manually, and then renormalized the edited weights by applying a computer program written for that purpose. For region 7, the edited, normalized weight field for the perturbed area is shown in the inset of Fig. 6.

After developing the regional weighting technique described here, the authors discovered that Hamill and Whitaker (2006b) used a very similar concept to formulate a special grid smoothing procedure for PQPFs produced with a reforecast analog model. While Hamill and Whitakers's application was also designed to remove artificial discontinuities along boundaries of PQPF subgrids and the weighting concept was similar to that underlying the application here, the specifics of the two methods differ in several respects.

5. Forecast performance with the overlapping-regions model

Regionally composited 6-h PQPFs were obtained by applying the overlapping-region regression equations and weighting procedure (ORG), described in the previous section, to warm and cool season independent samples noted in section 2b. For the example case discussed in section 3, the PQPF field obtained with the ORG model is shown in Fig. 3b. Comparing this figure with Fig. 3a, which contains the corresponding PQPF field obtained with the discrete regions model (DRG), we see that the artificial regional discontinuities have been eradicated. Otherwise, the two PQPF fields are remarkably similar. This gratifying finding was repeated in each of many other case comparisons that included both seasons, all forecast projections, and all precipitation thresholds.

The effectiveness of the ORG model in preventing artificial PQPF discontinuities was also examined objectively. In limited tests, the relative frequency distribution of the magnitude of the spatial probability gradient along common discrete regional boundaries (Fig. 4) was compared for ORG and DRG model PQPFs. The discrete regional boundaries from the Continental Divide

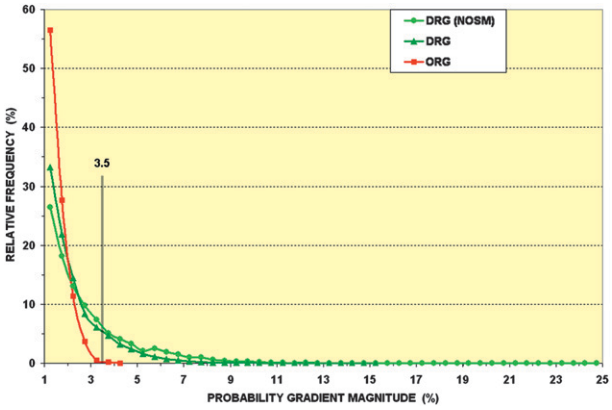

FIG. 7. Relative frequency of 6-h PQPF gradient magnitude (percent per 4-km grid interval) along discrete region boundaries east of the Continental Divide. The PQPFs are for the ≥0.10-in. exceedance threshold, 36-h forecast projection, 1200 UTC cycle, and eight full cool seasons. Probability gradient magnitudes less than one percent per grid interval were excluded from the samples; the 3.5% breakpoint is discussed in the text. DRG (NOSM) refers to discrete regions without probability smoothing.

westward were excluded in the comparative tests because true and artificial spatial PQPF gradients in this rugged mountainous region had very similar magnitudes.

Figure 7 shows probability gradient distributions for 36-h PQPFs for the ≥0.10-in. exceedance threshold, the 1200 UTC cycle, and the developmental sample consisting of all cool season days from 1 October 2001 to 31 March 2009 [1267 days (grids)]. Weak probability gradient magnitudes (<1%) were excluded from the relative frequency analyses as they are not relevant to the investigation. Also, in the case of the DRG model, two plots (with and without grid smoothing of the PQPF grids) are included to show that the grid smoothing (which was the same for DRG and ORG) had a relatively small impact on the frequency distributions. Note that the PQPF gradient distribution with the ORG model is strikingly different than that for the DRG model. In particular, only 0.21% of the PQPF gradient magnitudes (which appeared in only 12 of the 1267 grids) for ORG exceeded the arbitrary 3.5% breakpoint shown in Fig. 7, whereas 25.12% (which appeared in 597 grids) exceeded this breakpoint for DRG. These results support the claim made earlier that the regions-overlap and forecast-weighting techniques were effective at preventing artificial discontinuities wherever they occurred with the discrete regions model.

As noted earlier in this section, subjective examination of many cases indicated the prevention of PQPF discontinuities with the ORG model was accomplished without significantly modifying the ''true'' PQPF field (as exemplified in Fig. 3). This assessment was tested objectively on the basis of comparative PQPF performance scoring of ORG and DRG for full season independent samples. The performance measure was Brier score (Brier 1950; Wilks 1995) improvement on climatology (Brier skill score), where seasonal relative frequencies for the various predictand categories (described in section 2a) were used as the climatology surrogate.[7] As in Hamill and Whitaker (2006b), the Brier skill score for the grid area of concern was computed by summing the squared forecast error over all grid points in the area. While Hamill and Juras (2006a) point out that this computational procedure should overestimate the true Brier skill score for the area, head-to-head skill comparisons for PQPFs with similar statistical properties (the case here) should still be valid.

An example of the forecast skill comparisons is shown in Fig. 8a, which shows Brier skill scores for 6-h probabilities of multiple precipitation thresholds averaged over the full CONUS domain for the 30-, 36-, 42-, and 48-h projections (day 2) from the 1200 UTC model cycle. The scores are based on a cool season independent sample consisting of all days from the period 1 October 2007 to 31 March 2008. Figure 8a shows that the skill scores for ORG were at least as high as those with DRG for each precipitation threshold for the day 2 forecast lead time. Further, this result was true of any ''day'' of the full 3.5-day forecast period (see the introduction) and also the warm season (not shown). This finding indicates the removal of the artificial discontinuities was achieved without compromising forecast skill.

Recall (from section 2b) that the national approach (NAT) appears to be an acceptable alternative to the regionalized models for producing the gridded 6-h PQPFs. To examine its competitiveness with the regional models, comparative Brier skill scores for NAT are included in Fig. 8a. We see that the NAT skill scores are lower than those for ORG (and DRG), especially for the lighter precipitation thresholds, where event occurrences are more frequent.

To examine the comparative performance of ORG and NAT on a regional basis, Fig. 8b shows the day 2 skill scores, partitioned by the 13 discrete regions (Fig. 1), for the ≥0.25-in. precipitation threshold. (Corresponding regional scores for the DRG model were excluded from

[7] The monthly relative frequencies of 6-h precipitation noted in section 2a were also considered as a climatology surrogate. While these data provided a slightly better benchmark of the true climatology (they vary within a season and by time of the day, though their spatial resolution is weaker), these monthly relative frequencies were not available for the ≥0.01-in. precipitation threshold. Thus, we used the seasonal relative frequencies, as they were available for all precipitation thresholds.

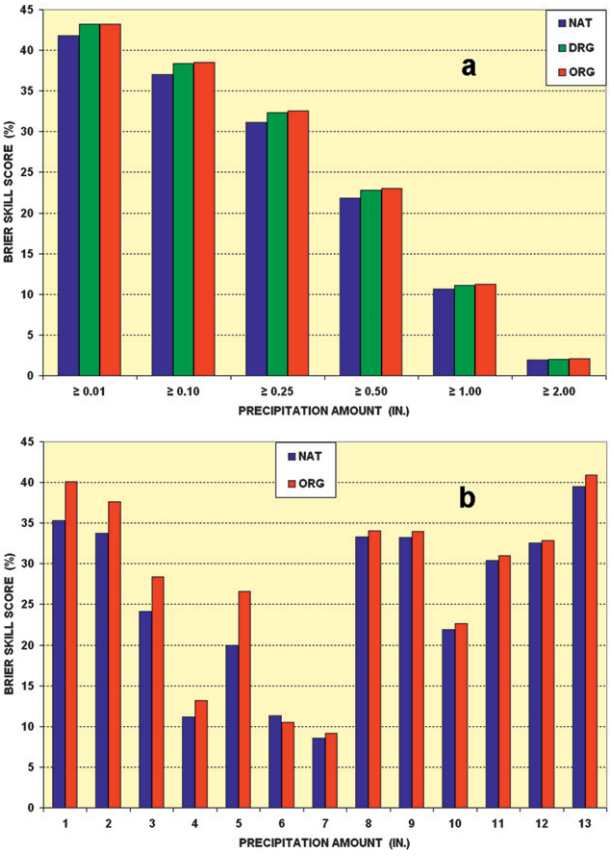

FIG. 8. Brier skill score (%) for 6-h PQPFs (a) over the CONUS domain with three models and (b) for individual regions at ≥0.25 in. with two models. The (cool season) scores are averaged over the 30-, 36-, 42-, and 48-h projections (day 2) from the 1200 UTC model cycle.

Fig. 8b because they were essentially the same as those for the ORG model, as indicated in Fig. 8a.) We find that for regions 1–5, which span the rugged mountainous western United States (Figs. 1 and 2a), the skill superiority of ORG was substantial. For the East (regions 8–13), on the other hand, the improvement of ORG on NAT was substantially less. Finally, for the high plains (regions 6 and 7), where much of the stage IV precipitation data were discarded because of the poor quality there (Fig. 3d), comparative skill with two methods was mixed.

Various properties of probability forecasts can be elucidated in probability reliability diagrams (Wilks 1995). Figure 9a contains reliability plots for 36-h probabilities of ≥0.25 and ≥1.00 in. with ORG and NAT for the full CONUS domain; Fig. 9b shows the number of cases corresponding to the plotted points. For ≥0.25 in., Fig. 9a shows that the ORG probabilities are slightly more reliable (most points are slightly closer to the perfect reliability line) than those for NAT. The corresponding comparison for ≥1.00 in. shows ORG with improved reliability and sharpness (peak probabilities are closer to 100%). Figure 9b shows that the sharpness with ORG was relatively strong for the ≥1.00-in. threshold, as peak probabilities for ORG fall in the 65%–75% interval versus the 45%–55% interval for NAT.

The reliability and probability distribution comparison for ORG and NAT is repeated for a very dry region (region 5) and a very wet region (region 1) in Figs. 9c and 9d. Here, we see improved reliability and sharpness for ORG over NAT for both ≥0.25 and ≥1.00 in. As for the full CONUS domain, the improved sharpness with ORG is stronger for the heavier precipitation threshold. These findings are consistent with ORG's substantial improvement in skill over NAT for these western regions, as shown in Fig. 8b.

It is noted that the reliability levels (in an absolute sense) of the ORG and NAT PQPFs in Figs. 9a and 9c are not particularly good. For instance, most of the upper probabilities showed a low bias, especially for the two western regions (Fig. 9c). This may be due to several factors, which include (a) the possible dissimilarity of statistical properties of the single season test sample to the multiseason developmental sample, (b) the inherent difficulty of estimating probabilities for such heavy precipitation amounts in a short (6 h) period, and (c) the possible interseasonal drift in the statistical properties of the samples over the span of the developmental and test periods. Recall that the test sample constituted the most recent season of the overall historical period.

6. Discussion

Forecast performance scores presented in the previous section indicate the ORG model was superior to the nonregionalized NAT model, especially in the mountainous western United States. From sections 3 and 4, on the other hand, we saw that extensive effort was expended to obtain "seamless" PQPF patterns over regional boundaries with the ORG approach. Also, the specification of the discrete and overlapping regions involved substantial experimentation. Further, the strong contrast in overlap for natural and quasi-arbitrary boundaries resulted in an artifact in the computed weights, which required manual removal. Thus, a question one may ask is: to what degree would the ORG PQPFs be degraded with reduced precision in the regions specification? In this section the question is addressed through sensitivity experiments carried out with "trimmed" versions of the ORG model.

The experiments were performed for the western United States in the area comprising regions 1–4 (Fig. 1), where the effort expended to define the discrete and

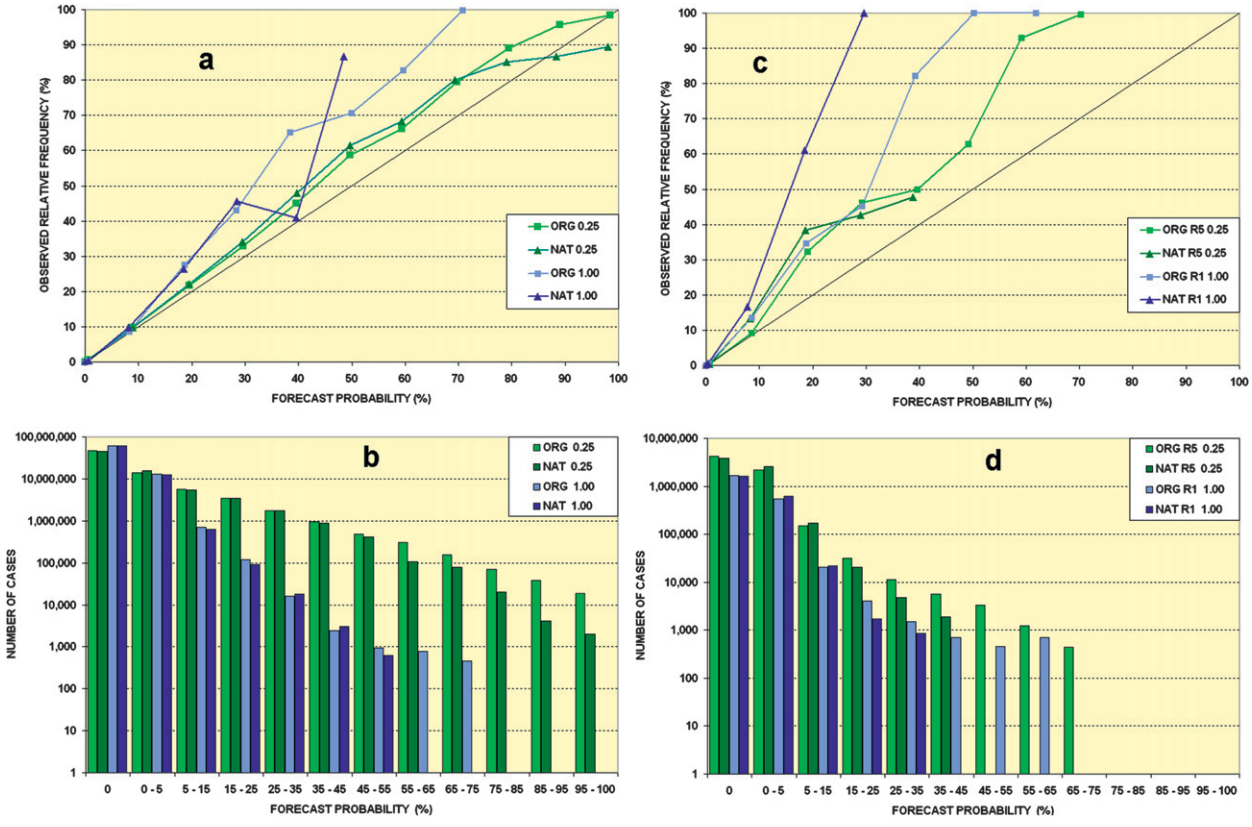

FIG. 9. Reliability of 36-h PQPFs of ≥0.25 and ≥1.00 in. with the ORG and NAT models for (a) the CONUS domain and (c) regions 1 and 5 (perfect reliability is indicated by the straight diagonal line). The abscissa values in these plots are mean probabilities within the (unequally spaced) intervals. The numbers of cases within the probability intervals in (a) and (c) are shown in (b) and (d), respectively (note the logarithmic ordinate scale). The models, regions, and precipitation thresholds (in.) are indicated in the legends.

overlap regions was greater than elsewhere (Fig. 4). In an experiment denoted "NO-RG," the four discrete regions were combined into one large region; the aim was to assess the (presumed) PQPF performance degradation that results from coarsening the regionalization in the ORG model in this western area. In another experiment, NO-TC, the original regionalization was retained, but all predictors involving the finescale topography and precipitation climatologies (TC) were excluded from the regression equation derivation. This experiment was intended to assess the degradation due solely to removal of the TC predictors. Finally, the experiment NO-RG-TC was designed to assess the degradation when the regionalization was coarsened and the TC predictors were withheld in the equation derivation.

For the example case used in this study, the PQPF fields for the western United States obtained with ORG and the three modified versions are shown in Fig. 10. Note that the PQPF field for NO-RG is quite similar that for ORG. On the other hand, the PQPF fields for NO-TC and NO-RG-TC exhibit a striking loss in spatial resolution. Also, the excessive spatial gradient in the probabilities along the Sierra–Cascade region (natural) boundary (Fig. 1) with the NO-TC model is unrealistic. It occurs because the boundary overlap there is very narrow (Fig. 4). (With no boundary overlap, the result would have been a discontinuity along a natural boundary!) These findings indicate that topoclimatic predictors had a central role in controlling the spatial gradients in the western United States, while the regionalization played a relatively small role. In fact, these predictors were also responsible for the fine spatial detail over the western United States that appeared even with the nonregionalized NAT model (Fig. 3c).

The comparative skill with the four models over the West for the four day 2 projections, based on the cool season independent sample noted in the previous section, is shown in Fig. 11. The relative skill among the ORG, NO-RG, and NO-TC models indicates the reduction in skill due to deregionalizing this area is fairly small, while the skill degradation stemming from removal of the topoclimatic predictors is large. Note also that the

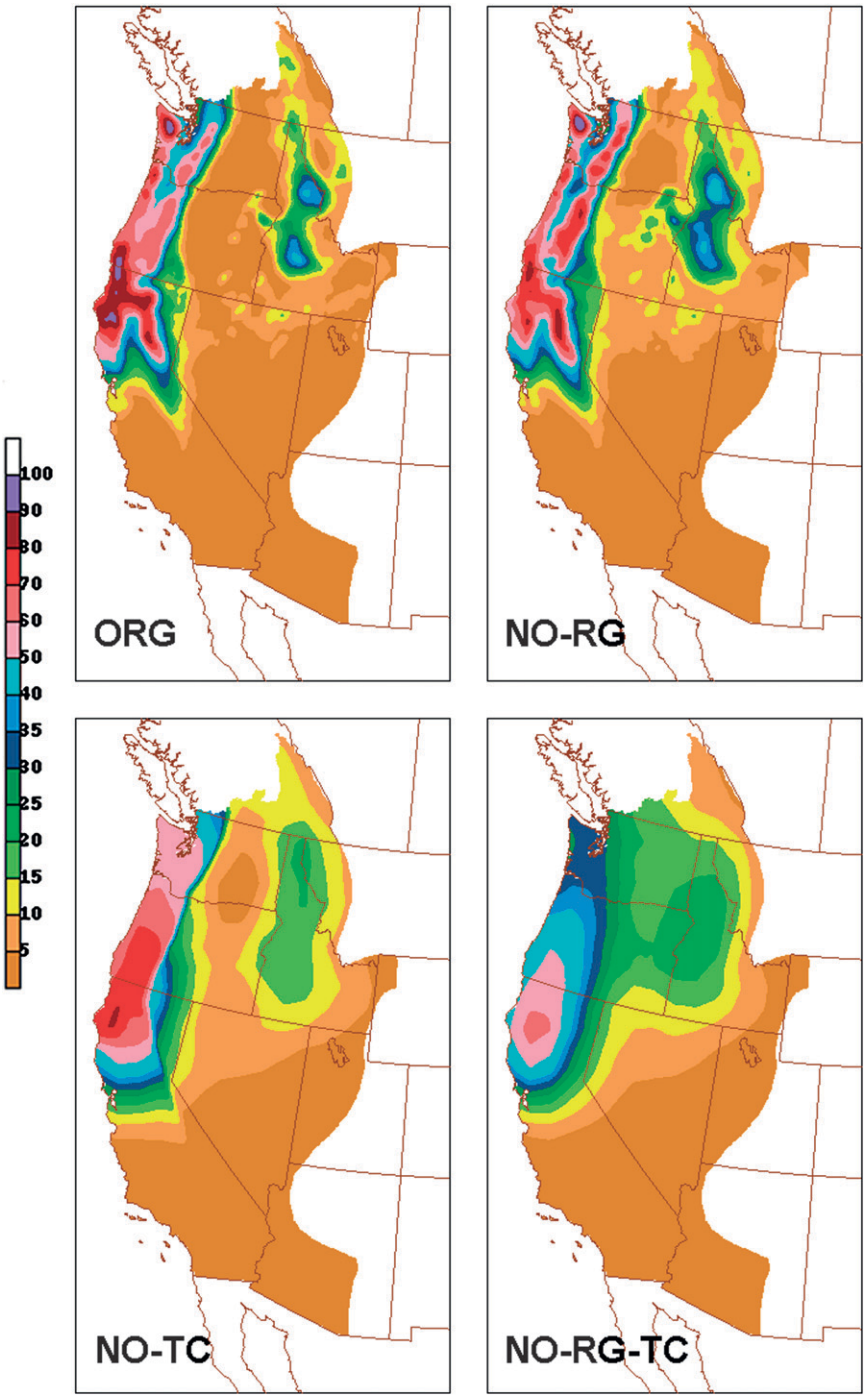

FIG. 10. Smoothed 36-h forecast probability (%) of ≥0.10 in. for the 6-h period ending 0000 UTC 30 Jan 2008 produced with four models over the western United States (composite of regions 1–4; see Fig. 1). The model abbreviations are ORG, overlapping regions; NO-RG, no regionalization; NO-TC, no topoclimatic predictors; and NO-RG-TC, no regionalization and no topoclimatic predictors.

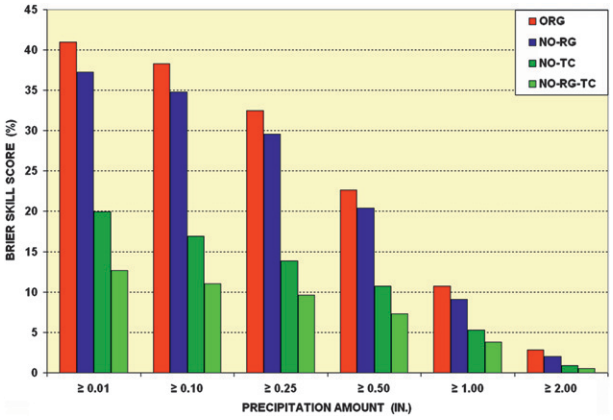

FIG. 11. Brier skill score (%) for 6-h PQPFs with four models over the western United States (composite of regions 1–4; see Fig. 1) averaged over the 30-, 36-, 42-, and 48-h projections (day 2) from the 1200 UTC model cycle.

reduction in skill due to deregionalization is greater when the topoclimatic predictors are not used than when they are included.

These findings, as well as those from the reliability diagrams in Fig. 9, indicate the primary role of the regionalization appears to be the enhancement of the calibration and sharpness of the probabilities. Spatial detail in the PQPFs, on the other hand, is largely controlled by the topoclimatic predictors, at least in areas of rugged mountainous terrain. This implies the precise specification of the regions was not critical to the quality of the precipitation probabilities. Still, the central findings in this study are that model regionalization improved the quality of the PQPFs, and that the regions-overlap and forecast-weighting techniques described herein effectively prevented artificial PQPF discontinuities along regional boundaries that would otherwise occur.

7. Summary and comments

In this study, we developed a method to treat the problem of nonmeteorological discontinuities in fine-grid 6-h probability forecasts of quantitative precipitation that appeared at boundaries of a conventionally regionalized MOS model. The treatment involved modifying the regionalization, whereby slight areal overlap among the regions was introduced by expanding the original nonoverlapping regions. The degree of overlap prescribed for a given region boundary varied depending on its meteorological significance. For a boundary where climatic precipitation contrasts across it were strong (weak), the overlap was relatively small (large). This principle supports strong spatial gradients in the precipitation probability forecasts along meteorologically significant (natural) regional boundaries and deters artificial gradients along insignificant regional boundaries.

With the adoption of the overlapping regions' technique, development of the prediction model followed the conventional regionalized MOS method. However, its application required blending multiple probability forecasts in the overlap zones, which was accomplished by weighting them with predetermined weighting constants. A weight constant for a point was directly related to its distance to the closest associated region boundary, and the sum of the multiple weights equals 1.0.

Subjective and objective forecast performance examinations with the overlapping regions model showed 1) that artificial discontinuities with the nonoverlapping regions model were eradicated, 2) the forecast skill was comparable to that for the latter model, and 3) the forecast performance properties were better than those for a nonregionalized model, especially in the mountainous western United States where many of the regional boundaries were natural boundaries.

While the overlapping regions technique to date has been applied only for QPF, the method may be applicable to other weather elements. Of course, the benefits achieved for another weather element will likely depend on the degree to which the regional overlap is customized to that element. In the present application the customization involved substantial experimentation, but subsequent sensitivity experiments indicated the quality of the forecasts was only weakly degraded when the regionalization was coarsened.

The technique used for weighting the multiple forecasts in region overlap zones was found to be robust for regions with assorted shapes and varying degrees of overlap. While a small perturbation in the weight field appeared for a unique overlap configuration, the flaw was not significant. Thus, the technique may have general applicability. In fact, the simple region-overlap and forecast weighting techniques described in this article may be applicable to the general problem of compositing local fine-mesh grids of data to form seamless map patterns in broad-area mosaics. A topic for future research is to test this notion on the basis of simulated local grids of varying shape and degrees of area overlap.

It is noted that a questionable aspect of the regionalization was subjectivity in the procedures used to specify the regions. The formulation of sound objective tools for specifying the overlapping and nonoverlapping regions should enhance future applications of the technique. An objective tool with potential merit involves computing performance scores at the individual grid points for forecasts from either a nonregionalized MOS model or from the NWP model used to drive the MOS model. Regardless of the scoring procedure, the

development of an objective technique to use such scoring grids to define regions suitable for gridded statistical forecast applications constitutes a formidable challenge.

Finally, we note that the 6-h PQPFs and other precipitation products derived from them have been produced in a real-time experimental mode from June 2008 to the present. The forecasts have been produced twice daily for projections in the 12–84-h range, but since April 2009 the forecasts have been extended to 192 h. Presently, the operational prototype QPF products are being evaluated; full operational deployment is expected in 2011.

Acknowledgments. Letitia Soulliard of the NCEP National Precipitation Verification Unit provided archives of the stage IV precipitation analyses. The questions and comments raised by the peer reviewers lead to substantial improvement in the clarity and scientific aspects of the article.

REFERENCES

Brier, G. W., 1950: Verification of forecasts expressed in terms of probability. *Mon. Wea. Rev.,* **78,** 1–3.

Carter, G. M., J. P. Dallavalle, and H. R. Glahn, 1989: Statistical forecasts based on the National Meteorological Center's numerical weather prediction system. *Wea. Forecasting,* **4,** 401–412.

Charba, J. P., 1977: Operational system for predicting thunderstorms two to six hours in advance. NOAA Tech. Memo. NWS TDL-64, 24 pp.

——, 1979: Two to six hour severe local storm probabilities: An operational forecasting system. *Mon. Wea. Rev.,* **107,** 268–282.

——, 1987: Zero-to-six and three-to-nine hour objective forecasts of heavy precipitation amount. NWS Tech. Procedures Bull. 370, 14 pp.

——, 1998: The LAMP QPF products. Part I: Model development. *Wea. Forecasting,* **13,** 934–965.

——, and F. Liang, 2005: Automated two-hour thunderstorm guidance forecasts. Preprints, *Conf. on Meteorological Applications of Lightning Data,* San Diego, CA, Amer. Meteor. Soc., 3.4. [Available online at http://ams.confex.com/ams/pdfpapers/84746.pdf.]

——, and F. G. Samplatsky, 2011: High-resolution GFS-based MOS quantitative precipitation forecasts on a 4-km grid. *Mon. Wea. Rev.,* **139,** 39–68.

——, Y. Lui, M. H. Hollar, B. Exley, and A. Belayachi, 1998: Gridded climatic monthly relative frequencies of precipitation amount for 1-, 3-, and 6-h periods over the conterminous United States. *Wea. Forecasting,* **13,** 25–57.

Daly, C., R. P. Neilson, and D. L. Phillips, 1994: A statistical topographic model for mapping climatological precipitation over mountainous terrain. *J. Appl. Meteor.,* **33,** 140–158.

Fulton, R. A., J. P. Breidenbach, D.-J. Seo, D. A. Miller, and T. O'Bannon, 1998: The WSR-88D rainfall algorithm. *Wea. Forecasting,* **13,** 377–395.

Glahn, H. R., and D. A. Lowry, 1972: The use of model output statistics (MOS) in objective weather forecasting. *J. Appl. Meteor.,* **11,** 1203–1211.

——, and D. Ruth, 2003: The new digital forecast database of the National Weather Service. *Bull. Amer. Meteor. Soc.,* **84,** 195–201.

——, K. Gilbert, R. Cosgrove, D. P. Ruth, and K. Sheets, 2009: The gridding of MOS. *Wea. Forecasting,* **24,** 520–529.

Hamill, T. M., and J. Juras, 2006a: Measuring forecast skill: Is it real skill or is it the varying climatology? *Quart. J. Roy. Meteor. Soc.,* **132,** 2905–2923.

——, and J. S. Whitaker, 2006b: Probabilistic quantitative precipitation forecasts based on reforecast analogs: Theory and application. *Mon. Wea. Rev.,* **134,** 3209–3229.

——, R. Hageborn, and J. S. Whitaker, 2008: Probabilistic forecast calibration using ECMWF and GFS ensemble reforecasts. Part II: Precipitation. *Mon. Wea. Rev.,* **136,** 2620–2632.

Henkel, A., and C. Peterson, 1996: Can deterministic quantitative precipitation forecasts in mountainous regions be specified in a rapid, climatologically consistent manner with Mountain Mapper functioning as the tool for mechanical specification? *Abstracts, Fifth National Heavy Precipitation Workshop,* State College, PA, NWS/NOAA, 31 pp. [Available from Office of Climate, Water, and Weather Services, W/OS, 1325 East-West Hwy., Silver Spring, MD 20910.]

Hughes, K. K., 1999: AVN-based statistical forecasts of thunderstorms and severe thunderstorms for the contiguous U.S. Preprints, *17th Conf. on Weather Analysis and Forecasting,* Denver, CO, Amer. Meteor. Soc., 201–205.

——, 2004: Probabilistic lightning forecast guidance for aviation. Preprints, *11th Conf. on Aviation, Range, and Aerospace/22th Conf. on Severe Local Storms,* Hyannis, MA, Amer. Meteor. Soc., 2.6. [Available online at http://ams.confex.com/ams/pdfpapers/81859.pdf.]

Iredell, M., and P. Caplan, 1997: Four-times-daily runs of the AVN model. NWS Tech. Procedures Bull. 442, 3 pp.

Kanamitsu, M., and Coauthors, 1991: Recent changes implemented into the Global Forecast System at NMC. *Wea. Forecasting,* **6,** 425–435.

Lowry, D. A., and H. R. Glahn, 1976: An operational model for forecasting probability of precipitation—PEATMOS PoP. *Mon. Wea. Rev.,* **104,** 221–232.

NWS, 2007: *NWS Focus*, 5 July 2007 (Special Edition), NWS Communications Office, Silver Spring, MD, 14 pp. [Available from NWS.Communications.Office@noaa.gov.]

Reap, R. M., 1991: Climatological characteristics and objective prediction of thunderstorms over Alaska. *Wea. Forecasting,* **6,** 309–319.

——, and D. S. Foster, 1979: Automated 12–36 hour probability forecasts of thunderstorms and severe local storms. *J. Appl. Meteor.,* **18,** 1304–1315.

Schaefer, T. J., 1990: The critical success index as an indicator of warning skill. *Wea. Forecasting,* **5,** 570–575.

Shuman, F. G., 1957: Numerical methods in weather prediction: II. Smoothing and filtering. *Mon. Wea. Rev.,* **85,** 357–361.

Wier, S., M. Mathewson, and T. J. LeFebvre, 1998: Grid editing for the Interactive Forecast Preparation System. Preprints, *14th Int. Conf. on Interactive Information and Processing Systems for Meteorology, Oceanography, and Hydrology,* Phoenix, AZ, Amer. Meteor. Soc., 469–473.

Wilks, D. S., 1995: *Statistical Methods in the Atmospheric Sciences*. Academic Press, 467 pp.